J. Ocean Univ. China (Oceanic and Coastal Sea Research)
DOI 10.1007/s11802-017-3057-6
ISSN 1672-5182, 2017 16 (1): 49-56
http://www.ouc.edu.cn/xbywb/
E-mail:xbywb@ouc.edu.cn

The Influence of the Corrosion Product Layer Generated on the High Strength Low-Alloy Steels Welded by Underwater Wet Welding with Stainless Steel Electrodes in Seawater

BAI Qiang[1), 2)], ZOU Yan[2), *], KONG Xiangfeng[1), 2)], GAO Yang[2)], DONG Sheng[1)], and ZHANG Wei[3)]

1) *College of Engineering*, *Ocean University of China*, *Qingdao* 266100, *P. R. China*
2) *Shandong Provincial Key Laboratory of Ocean Environment Monitoring Technology*, *Institute of Oceanographic Instrumentation*, *Shandong Academy of Sciences*, *Qingdao* 266100, *P. R. China*
3) *Qingdao Institute of Marine Corrosion*, *Qingdao* 266071, *P. R. China*

(Received November 2, 2015; revised October 8, 2016; accepted October 18, 2016)

Abstract The high strength low-alloy steels are welded by underwater wet welding with stainless steel electrodes. The microstructural and electrochemical corrosion study of base metal (BM), weld zone (WZ) and heat affected zone (HAZ) are carried out to understand the influence of the corrosion product layer generated on the high strength low-alloy steels welded by underwater wet welding with stainless steel electrodes, methods used including , potentiodynamic polarization, electrochemical impedance spectroscopy (EIS) and scanning electron microscope (SEM). The results indicate that the WZ acts as a cathode and there is no corrosion product on it throughout the immersion period in seawater. The HAZ and BM acts as anodes. The corrosion rates of the HAZ and BM change with the immersion time increasing. In the initial immersion period, the HAZ has the highest corrosion rate because it has a coarse tempered martensite structure and the BM exhibites a microstructure with very fine grains of ferrite and pearlite. After a period of immersion, the BM has the highest corrosion rate. The reason is that the corrosion product layer on the HAZ is dense and has a better protective property while that on the BM is loose and can not inhibit the diffusion of oxygen.

Key words underwater wet welding; corrosion rate; corrosion product; protective property

1 Introduction

Underwater wet welding is one important repairing and maintenance technology for the structures and facilities used in offshore and sub-sea, and it is also widely used for repair of components and structures damage caused by fatigue and mishandling in nuclear power plants (Lananowski, 2008).

During the welding process, a mixture of base material (BM) and welding rod is rapidly heated to a high temperature, and then cooled rapidly (Padilla *et al*., 2013). Phase changes with reprecipitation and grain growth occur as a result of the extreme temperature gradient during the joining process, which makes the microstructures and morpho logies different (Sadeghian *et al*., 2014). The corrosion properties of the weld may, therefore, vary considerably. Because of these series of process, the area of each coupon can be divided into three different areas, *i.e.*, the weld zone (WZ), the heat affected zone (HAZ) and BM. Deen *et al.* (2010) studied the microstructure and electrochemical behavior of low alloy steel weldment by optical microscopy, potentiodynamic polarization and linear polarization resistance (LPR) method. The results showed that WZ was found least corrosion resistant than BM and HAZ because acicular ferrite structure provided low corrosion resistance than allotrimorphic and widman-stätten ferrite. Basak *et al*. (2008) investigated the chemical reactivity of oxide-free weld joints made of thermo-hardened carbon steel in different electrolytes by chronopotentiometry, electrochemical impedance spectroscopy (EIS) and scanning electron microscopy (SEM). It was established that both the microstructure and the electrolyte composition dictated the electrochemical response of the different materials constituting weld joints in contact with the electrolyte. The widmanstätten-type structure of the weld material increased its dissolution resistance.

Besides the heat-input and cooling rate, the filler metal can also modify corrosion behavior (Cui and Lundin, 2007). The high strength low-alloy steel is the major material used for infrastructures in marine environments. At present, the strength and stability of the underwater welded joints need this material as BM cannot meet the specified requirements in many cases if there is no addition of ele-

* Corresponding author. Tel: 0086-532-82968311
E-mail: blcf@netease.com

ments like Cr, Ni and Mo in welding rod. In this case, the WZ has the property like stainless steel. Therefore, the dissimilar metals between different areas of the joint have different microstructures (Torkamany *et al*., 2012). The electrochemical potential differences yield and galvanic corrosion occurs between these two different materials. Fushimi *et al*. (2008) applied a multi-channel electrode technique to carbon steel welded with type-309 stainless steel immersed in artificial seawater and proved that the weldment and HAZ acted as a cathode and an anode, respectively. Wu *et al*. (2015) used optical microscope, X-ray diffraction, scanning electron microscope and potentiodynamic polarization to investigate the corrosion behavior of dissimilar metals between ferritic stainless steel and low carbon steel. Electrochemical corrosion test indicated that the corrosion potential of dissimilar joint fell in between ferritic stainless steel and low carbon steel, and that dissimilar joint had greatest corrosion current density which was attributed to the effect of galvanic corrosion.

The HAZ is usually considered to be the most sensitive area when the high strength low-alloy steel and stainless steel couple with each other. In fact, the corrosion activities of different areas in welded joint are related to the chemical composition and structure as well as other factors such as corrosion product because it can protect the steel surface from corrosive species through a physical blocking effect (Du *et al*., 2009). Bordbar *et al*. (2013) studied the relationship between the corrosion products layer and corrosion resistance of different zones of the welded joint and reported that the morphology of the corrosion products layer covering various zones of X70 pipe steel welded joint exhibited different protective effects. If the corrosion products layer was fine and dense, the charge transfer resistance had a maximum value.

In this work, the high strength low-alloy steel CCSE40 was chosen as BM because it has favorable property and has been used more and more widely all over the world. In order to keep the stability of producing high-quality welded joints, the stainless steel electrode was chosen as filler material and the WZ was stainless steel. Until recently, few studies have been made on the effect of the corrosion product layer on the corrosion behavior of the underwater wet welded joints, so the novelty of this work lies in the investigation of the corrosion electrochemical characteristics of different coupled materials of a underwater welded joint in the presence of corrosion products after a period of immersion in seawater. The reasons for the development of the corrosion behavior were analyzed.

2 Experimental

2.1 Parent Metal and Welding Process

The material under investigation was CCSE40 high strength low-alloy steel plate with 25 mm thickness welded with V-shape of the weld pool by underwater manual welding. The cross-section schematic of the welded joint is shown in Fig.1. The filler material is stainless steel electrode. The chemical composition of BM, WZ, filler material and welding parameters are given in Tables 1 and 2 respectively. Multi-pass welding was applied to complete the joint. The underwater welding was carried out in tank of the size 2 m×3 m×3 m. The tank was filled with seawater, the depth being 2 m.

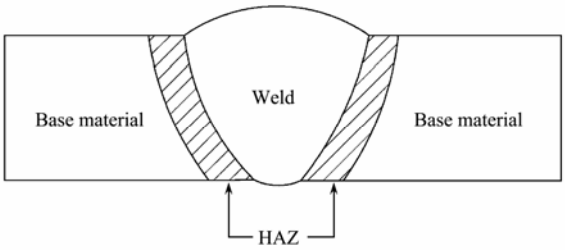

Fig.1 Cross-section schematic of the welded joint.

Table 1 Chemical compositions in wt.% of base metal and weld zone

Chemical composition	C	Mn	Si	S	P	Mo	Ni	Cr	Fe
Base metal	0.18	1.2	0.50	0.035	0.035	0.08	0.40	0.20	Balance
Weld metal	0.10	1.6	0.78	0.020	0.020	4.50	22.50	20.60	Balance

Table 2 Welding process parameters for underwater manual welding

Welding process	Power (w)	Voltage (V)	Current (A)	Welding speed (mm s^{-1})
Underwater manual welding	6400	33	192	2.5

2.2 Metallography, Surface Topography and Scanning Electron Microscope

Metallographic observations were carried out using GX-51 Olympus metallurgical microscopy. A 10 mm×30 mm ×10 mm specimen was obtained from the welded plate com- posed of BM, WZ and HAZ. After being ground with SiC abrasive paper and polished to a mirror finish (1 μm), this weldment sample was immersed in the etching solution. Because of the different corrosion resistance, two etchants were used to reveal the microstructure of the joint. The etching of BM and HAZ was carried out using 3% Nital solutions (3 mL nitric acid (HNO_3), 97 mL ethanol). Then the microstructure of WZ was etched by the solution made of 5 g $CuSO_4$, 20 mL hydrochloric acid and 20 mL distilled water.

The surface topography was observed by IXUS 80 camera. The coupons which included WZ, HAZ and BM were photographed when they were taken out of the seawater immediately after immersion for a period of time. Then, the loose corrosion products were scraped off using

a coarse wire brush and the coupons were photographed again.

The microstructural observations of corrosion product were carried out using Philips XL30 scanning electron microscope (SEM).

2.3 Electrochemical Measurements

The coupons for electrochemical measurements were cut into different pieces by mechanical sawing to separate the WZ, HAZ, and BM. Any transitional area between the different zones was avoided. Because the cooling rate of underwater welding is much faster than that of welding in air (Maksimov, 2010), the width of the HAZ is only 0.2 cm. All of the coupons were rearranged in the original location and embedded in epoxy resin to be used as working electrodes (WE). The WE was polished with metallurgical paper up to No.1000 grade, and cleaned with acetone. After polishing, the exposed area was 1 cm^2, 0.2 cm^2, and 1 cm^2 for WZ, HAZ, and BM, respectively. Then, the coupons were coupled with each other and immersed in seawater which was from Huiquan Bay of Qingdao, filtrated before tests, static in the chest and replaced every week. The volume of the seawater was 10 L. The average room temperature was 20℃.

Electrochemical measurement was implemented with a PARSTAT 2263 potentiostat/galvanostat electrochemical system equipped with Powersuite software. The electrochemical measurements were performed in a three-electrode setup consisting of a test sample used as WE, a platinum grid as auxiliary electrode (AE) and a saturated calomel electrode as reference (RE). At first, open circuit potential (OCP) of the coupled electrode (CE) was obtained. And then, different zones of welded joint were break down and the same electrochemical test plus electrochemical impedance spectroscopy (EIS) and potentiodynamic polarization curves plotting were performed. EIS measurement frequency was selected to be in the range of 100 kHz to 10 MHz with an applied AC perturbbation of 10 mV relative to the coupled potential. The ZView impedance analysis software was used to fit the achieved data. The polarization curves potential ranges were −400 – +400 mV (*vs.* E_{corr}) with a scan rate of 0.5 mV s^{-1}. The obtained data were analyzed by Corrview software. All electrochemical tests were duplicated three times at room temperature.

3 Results and Discussion

3.1 Surface Topography

Fig.2a shows the surface topography of underwater wet welded joints after immersion in seawater for 48 weeks. It is clear that no corrosion is observed on the WZ, and the rust layer is formed on the HAZ and BM. This means that the WZ is cathode while the HAZ and BM are anodes. Scraping off the rust layer, it could be found that the rust layer on the BM is looser and easily be removed. But most areas of the HAZ are covered by the black and compact rust layer (Fig.2b). It is difficult to be scraped off.

3.2 Microstructure Analysis

Underwater wet welded joints microstructures generally are composed of a complex mixture of microstructural constituents. An etched surface of the BM is shown in Fig.3a, where a fine-grained ferrite (light area) and pearlite phase (dark area) can be seen. The width of the HAZ is 2 mm. The grain size of HAZ increases for the thermal circle associated with welding. Therefore, the HAZ has a coarse tempered martensite structure and some carbide precipitates along the original austenite grain boundary (Fig.3b). The WZ microstructure consists of austenitic structure and ferrite (Fig.3c). These three zones show different microstructures which can cause various electrochemical properties.

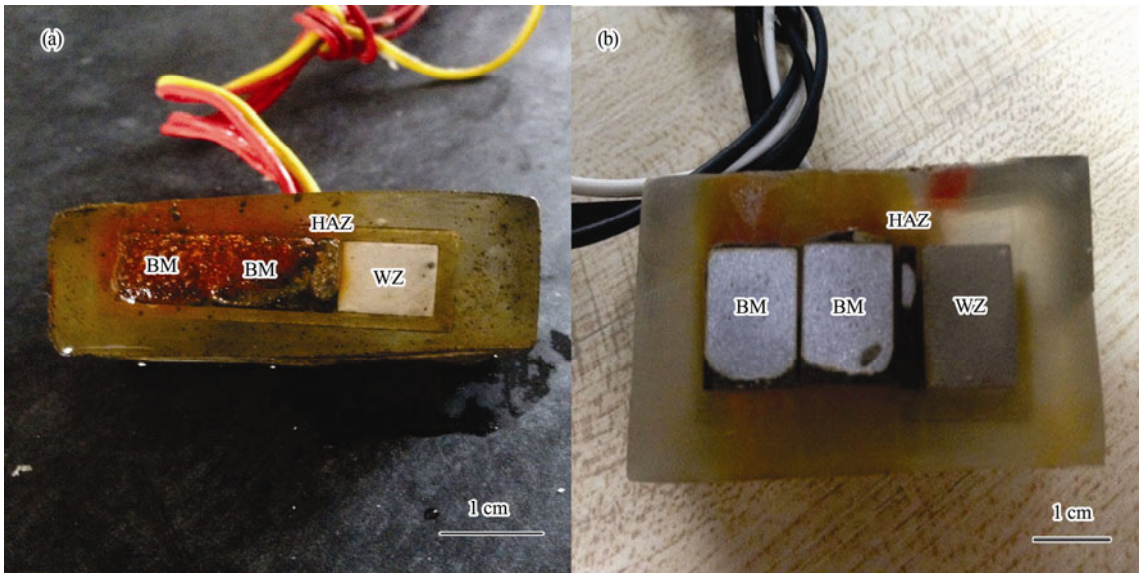

Fig.2 Surface topography of underwater wet welded joints after immersion in seawater for 48 weeks. a) before scraping off the loose corrosion products, and b) after scraping off the loose corrosion products.

Fig.3 Microstructures of a) BM, b) HAZ, and c) WZ.

3.3 Open Circuit Potential

The OCP of different zones of underwater wet welded joint is monitored as a function of immersion time in seawater. The potentials on the BM, WZ, HAZ and CE are shown in Fig.4. The WZ has the most positive OCP while the BM has the most negative OCP. The OCP of the BM is almost the same as that of the CE and it is appreciably more negative than that of the HAZ. The potential difference between the WZ and BM becomes smaller as a function of immersion time. The OCP evolution shows that the weld material has a more cathodic potential compared to the base carbon steel and HAZ. This means that the weld is less active compared to BM and HAZ and there is thus a risk of galvanic coupling in the case of coupled welded joints. WZ has nobler corrosion potential as negative electrode, while HAZ and BM have lower potentials as positive electrode, hence galvanic couple forms.

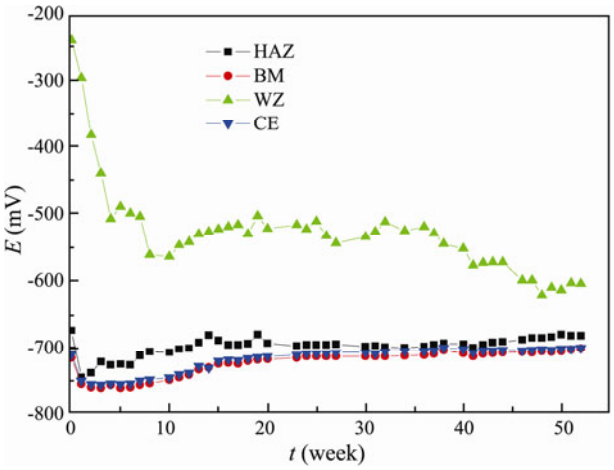

Fig.4 Open circuit potential of different zones of underwater wet welded joint in seawater as a function of immersion time.

3.4 Potentiodynamic Polarization Scans

Potentiodynamic polarization curves are obtained after the coupons immersion in seawater for a period of time. The WZ exhibits anodic passivity (Fig.5) during the corrosion process, whereas the HAZ and BM have typical characteristics of active dissolution at the first immersion time in seawater (Figs.5c and 5d). During the whole immersion period, the corrosion rate of the WZ is lowest compared with those of the HAZ and BM. At the first immersion period (Fig.5a), the cathodic part of the polarization curve is attributed to the limiting current density which may be determined by diffusion controlled oxygen reduction reaction for BM and HAZ. The cathodic current density of the HAZ is larger than that of the BM. With immersion time increasing (Fig.5b), the corrosion products are formed on the HAZ and BM. They can be reduced in the potential range of the oxygen reduction (Zou *et al*., 2011). The cathodic process is controlled by the mixture of the oxygen reduction and the reduction of the corrosion products. The cathodic Tafel slopes decrease. As the corrosion product layer grows thicker (Figs.5c and 5d), the anodic Tafel slopes increase because the corrosion product acts like a physical barrier against ferrous ions diffusion. The corrosion rate of the BM is larger than that of the HAZ. During the corrosion process, the WZ has the lowest corrosion rate and acts as cathode all the time. At the initial immersion time, the HAZ has the highest corrosion rate. With increasing of exposure time and growth of corrosion product layer, the BM has the highest corrosion rate.

3.5 Electrochemical Impedance Spectroscopy Measurements

From the polarization curves, it can be concluded that it is the corrosion product layer that influences the corrosion behavior of the different zones of the underwater welded joint. Because there is no corrosion product on the WZ, the EIS of the HAZ and BM are performed only in order to study the corrosion product effect on the corrosion behavior.

Fig.6 shows the Nyquist diagrams of HAZ and BM of the underwater welded joint after immersion in seawater for various periods as results of EIS tests. The shapes of the HAZ and BM in Fig.6a and Fig.6b seem almost the same in the initial immersion time, which indicates that these two areas have similar corrosion behavior. After immersion in seawater for 20 weeks (Fig.6c and Fig.6d), the Nyquist diagrams of the HAZ include a diffusion tail in the low-frequency region while that of BM does not have it. The HAZ and BM exhibite different corrosion behavior.

According to the Nyquist diagrams and the growth of the

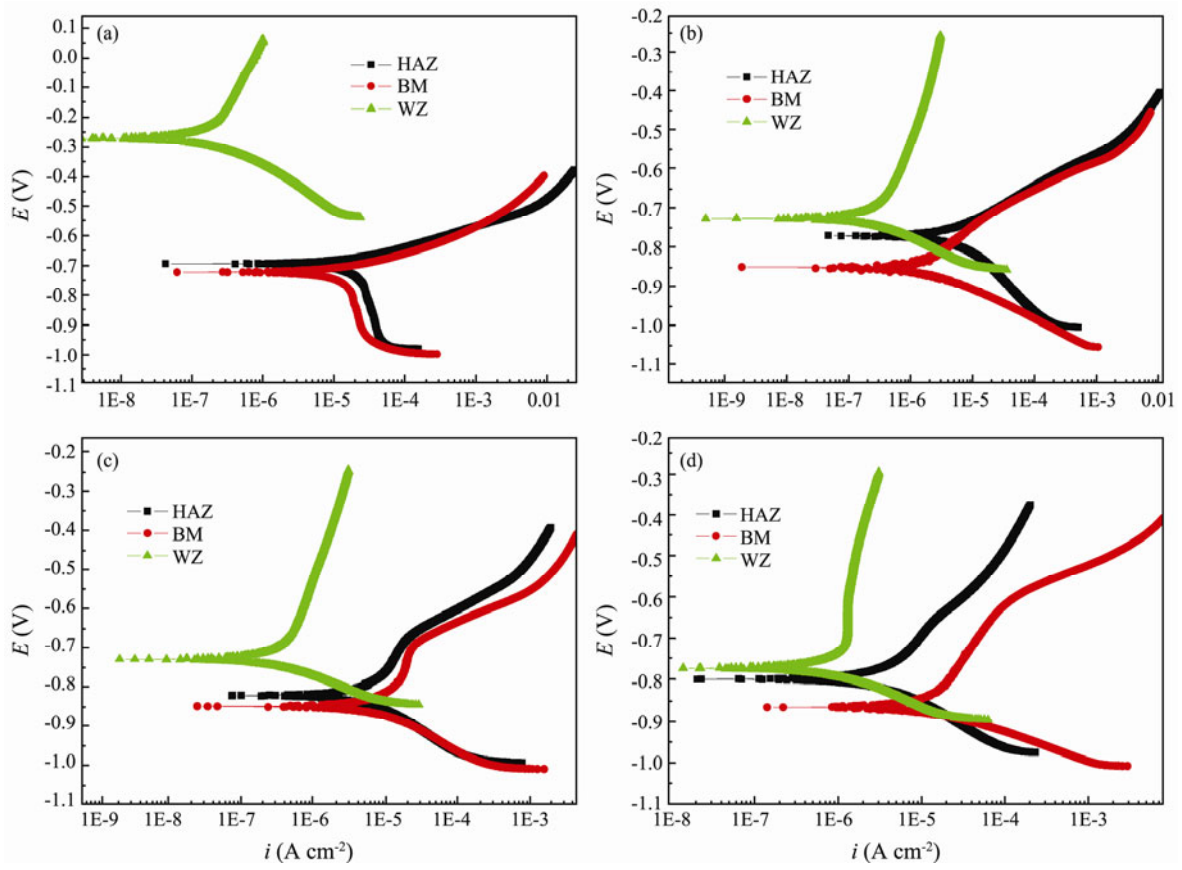

Fig.5 Polarization diagrams for the BM, WZ and HAZ after immersion in seawater for various time periods: a) 0.5 h, b) 8 weeks, c) 24 weeks, and d) 52 weeks.

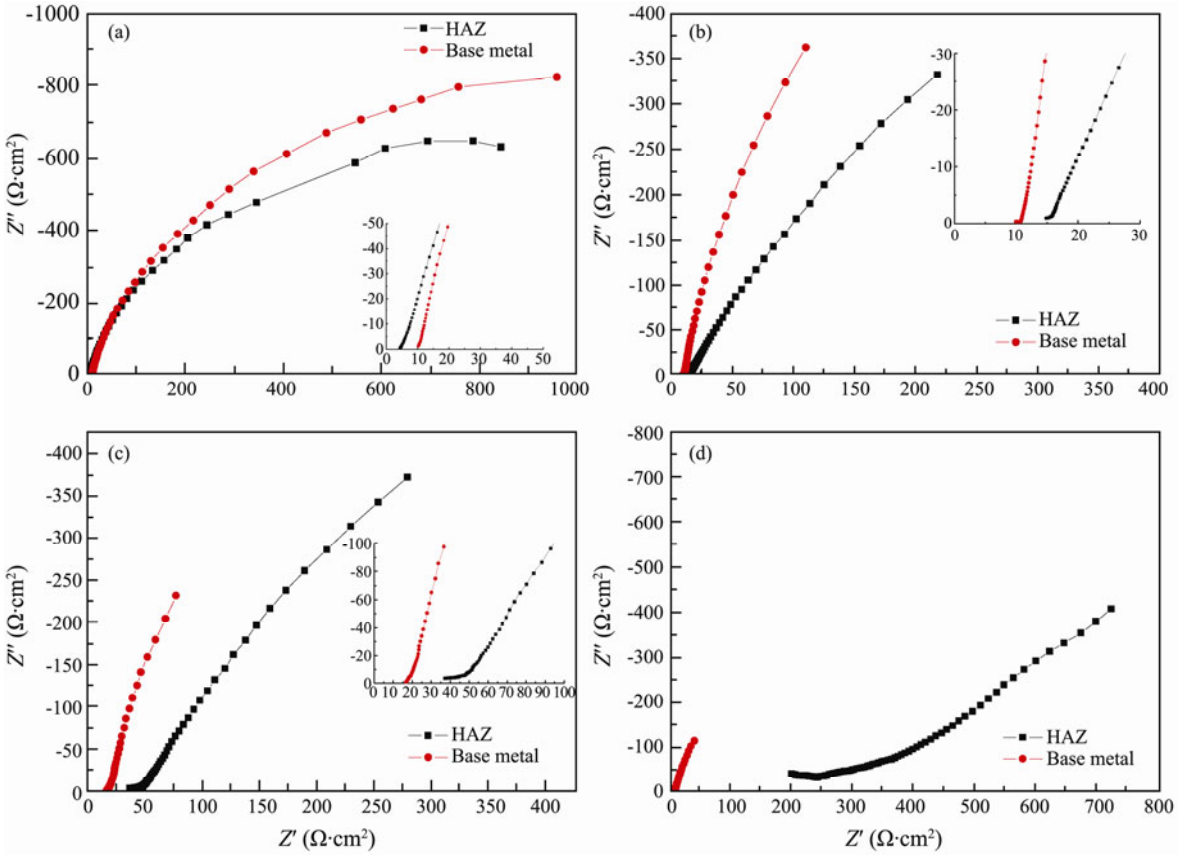

Fig.6 The Nyquist diagrams of the BM and HAZ after immersion in seawater for various time periods: a) 1 week, b) 12 weeks, c) 20 weeks, and d) 52 weeks.

corrosion product, the equivalent circuit can be concluded. During the initial period (before 12 weeks), the corrosion product layer is thin and loose. It cannot protect the metal and the influence of the corrosion product can be ignored. The Nyquist diagrams have only one semicircle and the equivalent circuit can be proposed and depicted in Fig.7a. After this period (from 12 weeks to 20 weeks), the corrosion product layer becomes thicker and it can prevent a part of the oxygen. The Nyquist diagrams illustrate two compressed semicircles and the proposed equivalent circuit used to fit the experimental data is shown in Fig.7b (Zou *et al*., 2010). After immersion for 20 weeks, the corrosion product layer of the HAZ is compact and the impedance diagrams seem to be markedly influenced by diffusion processes. The equivalent circuit of the HAZ can be described in Fig.7c (Bordbar *et al*., 2013). The Nyquist diagrams of the BM exhibite two semicircles and the equivalent circuit is still shown in Fig.7b. In the equivalent circuit, R_s denotes solution resistance, R_f is the film resistance due to the formation of corrosion products, R_{ct} is the charge transfer resistance, W is Warburg impedance (diffusion parameter), C_f is the electrical capacity of the corrosion products layer and Q_{dl} is constant phase element (CPE) at the double layer.

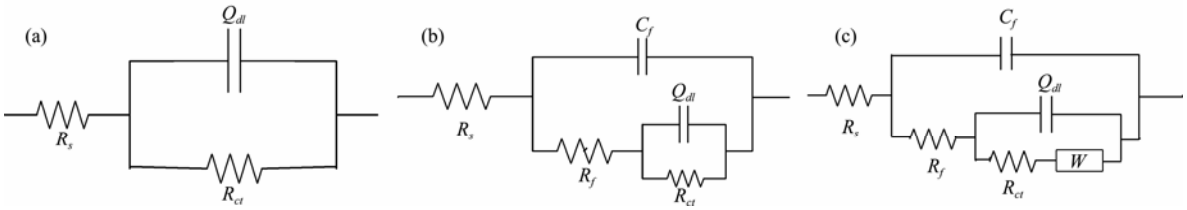

Fig.7 The equivalent circuit proposed for the electrochemical impedance response: a) before 12 weeks, b) from 12 weeks to 20 weeks, and c) after 20 weeks for HAZ.

The rust layer resistance R_f, deduced from extrapolation to the real axis of the semicircle of the high frequencies, represents the barrier against migration of oxygen in association with the corrosion reaction and is the most useful for estimating the protective properties of the rust layers (Ito *et al*., 1988). Fig.8 shows the variations of the R_f and R_{ct} as a function of exposure time. The R_f values for the corrosion product layer of the HAZ remarkably increase with exposure time while those of the BM are almost unchanged (Fig.8a). According to Wang *et al*. (1997), the more protective the rust layer is, the higher the value of R_f. Therefore, the corrosion product layer on the HAZ becomes dense prolong with the immersion time and inhibites the permeation of the oxygen, leading to better protective effect while that on the BM can not play this role. As reflected by R_{ct} (Fig.8b), the values of the HAZ increase significantly and those of the BM decrease slightly.

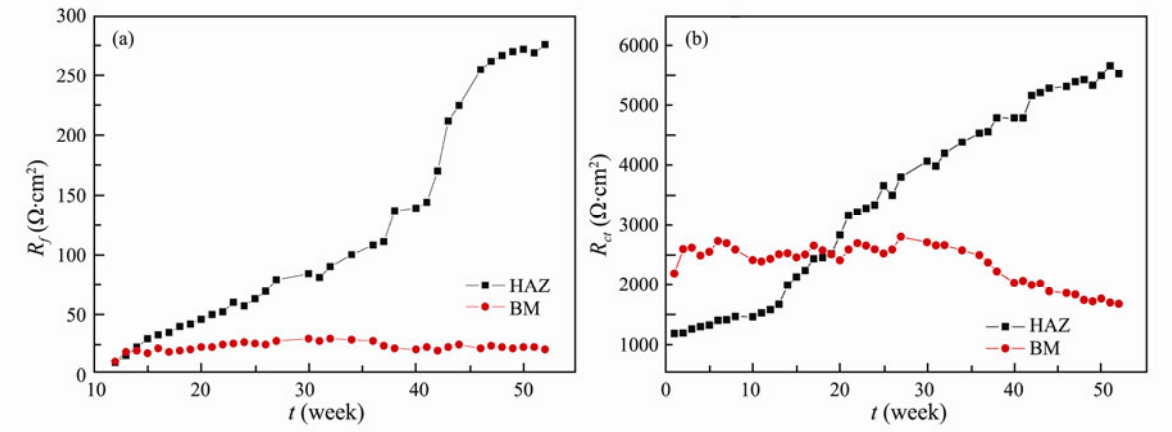

Fig.8 The variation of the a) corrosion product resistance, and b) charge transfer resistance of the HAZ and BM.

3.6 SEM Observation of the Corrosion Product Layer

According to the analysis of EIS, the corrosion product layers on the HAZ and BM are different which cause dissimilar corrosion behavior. In this case, the microstructure of the corrosion product is studied by SEM. Fig.9 shows the SEM images of the corrosion products layer generated on the different zones of underwater welded joint surfaces after 52 weeks immersion in seawater. As can be seen from the picture, the HAZ indicates a dense corrosion product layer with small cracks (Fig.9a) and the BM shows big porosities (Fig.9b). Although the corrosion product layer generated on the HAZ has some cracks, it is more compact and impermeable than that of the BM. This observation confirms that the HAZ has the maximum corrosion resistance and the minimum corrosion rate in comparison with the BM after immersion in seawater for a period of time because of the protection of the dense corrosion product layer.

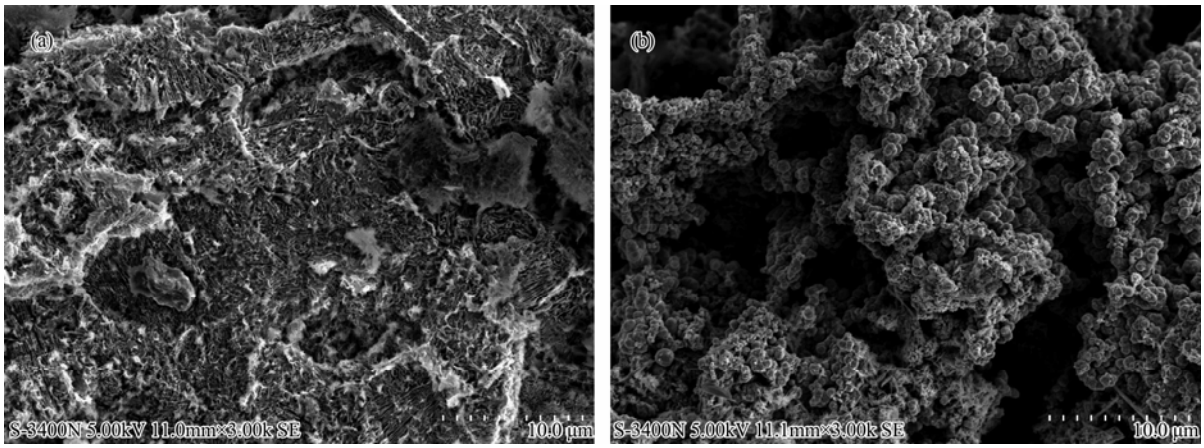

Fig.9 The SEM micrographs of the corrosion product layer generated on underwater welded joint surfaces after immersion in seawater for 52 weeks: a) HAZ, and b) BM.

3.7 Corrosion Mechanism

Corrosion of the underwater welded joints in seawater is a complex system with multiple electrodes. Differences in composition and microstructure in a WZ relative to HAZ or BM can create an electrochemical potential between the zones and cause galvanic corrosion. Consequently, the corrosion behavior in different zones is different in corrosive media. Due to different corrosion activitiy in different zones, the corrosion product layers with different thicknesses and protective properties are formed on the welded joint (Zhang and Cheng, 2009). There points can affect the corrosion behavior of the different coupled materials of the underwater welded joint in seawater.

From analysis of microstructure, the WZ microstructure consists of austenitic structure and ferrite. The BM exhibites a microstructure with very fine grains of ferrite and pearlite. The HAZ has a coarse tempered martensite structure. These structural characteristics cause the phenomenon that the WZ has the best corrosion-resistance and the HAZ has the worst corrosion-resistance at the initial stage of immersion.

From analysis of chemical composition, there is a large amount of Cr and Ni in welded metal and the property is similar to that of stainless steel. The HAZ and BM are of high strength low-alloy steel. The difference of the chemical composition makes the WZ have the most positive OCP, the less electrochemical activity compared to HAZ or BM and exhibite anodic passivity. Therefore, the WZ act as cathode and there is no corrosion on it during the entire immersion time.

When the welded joint is immersed in seawater, the HAZ and BM begin to be attacked by the aggressive ions and the corrosion product begins to form on these two areas. In the initial period of immersion, the corrosion product is quite permeable due to their loose and porous structure (Yamaguchi *et al*., 1994). The corrosion reaction is controlled by the reduction of the dissolved oxygen which is easy to diffuse through rust layers during this period. The HAZ shows a higher corrosion rate compared to the BM and WZ due to its microstructure. After a period of immersion, the corrosion product layers of the HAZ and BM have different thicknesses and protective properties because of their different structure. The corrosion product of the BM is loose and includes big porosities. The dissolved oxygen can easily diffuse to the surface of the metal. The corrosion resistance calculateby EIS decreases little with the extension of the immersion time. The corrosion product layer of the HAZ is dense and compact, which can protect the steel surface from corrosive species through a physical blocking effect (Du *et al*., 2009). As a result, the corrosion resistance increases and the corrosion rate decreases. In this process, the struture of the corrosion product layer plays an essential role in the corrosion mode of the steel.

4 Conclusions

In this work, the influence of the corrosion product layer on the corrosion behavior of the high strength low-alloy steels welded by underwater wet welding with stainless steel electrodes in seawater is discussed and the following conclusions are obtained:

1) In seawater, the WZ acts as a cathode and there is no corrosion on it throughout the immersion period. In the initial immersion period, the HAZ has the highest corrosion rate. After a period of immersion, the BM has the highest corrosion rate.

2) The WZ microstructure consists of austenitic structure and ferrite. The BM exhibites a microstructure with very fine grains of ferrite and pearlite. The HAZ has a coarse tempered martensite structure. These structural characteristics lead to the phenomenon that the HAZ is the most susceptible area to corrosion at the initial immersion period.

3) The HAZ has a dense corrosion product layer and the BM has big porosities. Therefore, the R_f of the HAZ increases significantly as a function of immersion time while that of the BM remains almost unchanged, which means that the corrosion product of the HAZ has a better protective property than that of the BM. As a result, the corrosion rate of the BM is larger and the corrosion resistance is smaller than those of the HAZ after a period of

immersion.

Acknowledgements

The authors appreciate the financial support by the National Natural Science Foundation of China (Nos. 5120 9129 and 21203034).

References

Basak, A. K., Diomidis, N., Celis, J. P., Masquelier, C., and Warichet, D., 2008. Chemical reactivity of thermo-hardenable steel weld joints investigated by electrochemical impedance spectroscopy. *Electrochimica Acta*, **53**: 7575-7582.

Bordbar, S., Alizadeh, M., and Hashemi, S. H., 2013. Effects of microstructure alteration on corrosion behavior of welded joint in API X70 pipeline steel. *Materials and Design*, **45**: 597-604.

Cui, Y., and Lundin, C. D., 2007. Austenite-preferential corrosion attack in 316 austenitic stainless steel weld metals. *Materials and Design*, **28**: 324-328.

Deen, K. M., Ahmad, R., Khan, I. H., and Farahat, Z., 2010. Microstructural study and electrochemical behavior of low alloy steel weldment. *Materials and Design*, **31**: 3051-3055.

Du, C., Li, X., Liang, P., Liu, Z., Jia, G., and Cheng, Y., 2009. Effects of microstructure on corrosion of X70 pipe steel in an alkaline soil. *Journal of Materials Engineering and Perfomance*, **18**: 216-220.

Fushimi, K., Naganuma, A., Azumi, K., and Kawahara, Y., 2008. Current distribution during galvanic corrosion of carbon steel welded with type-309 stainless steel in NaCl solution. *Corrosion Science*, **50**: 903-911.

Ito, S., Kihira, H., and Murat, T., 1988. A new method to monitor in-situ protective properties of rust on weathering steel. In: *American Society for Testing and Materials*. Dean, S. W., and Lee, T. S., eds., ASTM STP 965, Philadelphia PA, 366-373.

Lananowski, J., 2008. Development of under-water welding techniques. *Welding International*, **25**: 933-937.

Maksimov, S. Y., 2010. Underwater arc welding of higher strength low-alloy steels. *Welding International*, **24**: 449-454.

Padilla, E., Chawla, N., Silva, L. F., dos Santos, V. R., and Paciornik, S., 2013. Image analysis of cracks in the weld metal of a wet welded steel joint by three dimensional (3D) X-ray microtomography. *Materials Characterization*, **83**: 139-144.

Sadeghian, M., Shamanian, M., and Shafyei, A., 2014. Effect of heat input on microstructure and mechanical properties of dissimilar joints between super duplex stainless steel and high strength low alloy steel. *Materials and Design*, **60**: 678-684.

Torkamany, M. J., Sabbaghzadeh, J., and Hamedi, M. J., 2012. Effect of laser welding mode on the microstructure and mechanical performance of dissimilar laser spot welds between low carbon and austenitic stainless steels. *Materials and Design*, **34**: 666-672.

Wang, H., Wei, F. I., Chang, Y. S., and Shih, H. C., 1997. The corrosion mechanisms of carbon steel and weathering steel in SO_2 polluted atmospheres. *Materials Chemistry and Physics*, **47**: 1-8.

Wu, W. Y., Hu, S. S., and Shen, J. Q., 2015. Microstructure, mechanical properties and corrosion behavior of laser welded dissimilar joints between ferritic stainless steel and carbon steel. *Materials and Design*, **65**: 855-861.

Yamaguchi, S., Yoshida, T., and Saito, T., 1994. Improvement in descaling of hot strip by hydrochloric acid. *Isij International*, **34**: 670-678.

Zhang, G., and Cheng, Y., 2009. Micro-electrochemical characterization of corrosion of welded X70 pipeline steel in near-neutral pH solution. *Corrosion Science*, **51**: 1714-1724.

Zou, Y., Wang, J., and Zheng, Y. Y., 2010. Characteristics of the electrode process for rusted carbon steel. *Acta Physico-Chimica Sinica*, **26**: 2361-2368.

Zou, Y., Wang, J., and Zheng, Y. Y., 2011. Electrochemical techniques for determining corrosion rate of rusted steel in seawater. *Corrosion Science*, **53**: 208-216.

(Edited by Xie Jun)